# Wave propagation modeling in heterogeneous, porous media

Ana Beatriz A. QUINTAL*, Viatcheslav I. PRIIMENKO, LENEP/UENF, Djalma M. SOARES FILHO, CENPES/PETROBRAS



## Abstract

Biot's equations are used for modeling wave propagation in 2-D heterogeneous porous media through a second-order accurate time, fourth-order accurate space, staggered-grid finite-difference scheme, based on Madariaga-Virieux formulation. For implementing the numerical scheme, Biot's equations are reformulated into a first-order system of four equations of motion and four constitutive equations, expressed explicitly in particle-velocity components, stresses and pore-fluid pressure. Results from poroelastic and an equivalent Levander's elastic modeling are compared to illustrate Biot's poroelastic effect and then the amount of additional information available for seismic and sonic inversion.

## Introduction

The theory of poroelasticity developed by Biot (1962) is a solution to the problem of elastic wave propagation in fluid-saturated porous media. It has been used to compute the seismic response of fluid-saturated reservoirs by numerical implementation of a 2-D finite-difference scheme (Hassanzadeh, 1991; Zhu and McMechan, 1991; Dai et al., 1995).

Following Levander (1988) for the elastic equations, we reformulate Biot's equations for heterogeneous, poroelastic media into a first-order system of four coupled equations of motion expressed explicitly in terms of velocity components of the solid and of the fluid relative to the solid, and four constitutive equations expressed explicitly in terms of stress components and pore-fluid pressure component. Explicitly expressing stresses and pore-fluid pressure, makes relatively simple to implement numerically the source function and to satisfy free-surface boundary conditions.

Then, a second-order accurate time, fourth-order accurate space, 2-D staggered-grid finite-difference scheme, based on Madariaga-Virieux formulation (Madariaga, 1976; Virieux, 1984, 1986), is implemented to the first-order system of equations in order to simulate wave propagation in heterogeneous poroelastic media. In specific conditions, the slow wave is observed, in addition to the ordinary compressional wave and the shear wave.

Computations from poroelastic and an equivalent Levander's elastic modeling are performed and compared, both in seismic and sonic ranges of frequencies. The results show primary and converted reflections from fluid and lithologic contacts, illustrating the effect of Biot's poroelasticity, and then the amount of additional information available for seismic and sonic inversion.

## Poroelastic theory

Biot's (1962) theory of poroelasticity describes elastic wave propagation in fluid-saturated porous media. It takes account of attenuation due to relative motion between a viscous pore fluid and the solid matrix. But the attenuation mechanism of this theory is not perfect; there are other factors that cause acoustic wave attenuation. Mavko and Nur (1975; 1979) and O'Connell and Budiansky (1977) suggested the squirt flow mechanism, which takes into account the attenuation caused by lateral fluid flow. In addition, the solid constituent is not completely elastic. However, Biot's theory is useful in petroleum exploration as it links the acoustic signals to reservoir parameters, such as porosity and permeability (Rosenbaum, 1974), and its limitations should be better understood. Besides, providing accurate and stable solutions to Biot's theory, represents an important step towards numerical computations for the BISQ model, that is, the unified Biot and squirt flow mechanism (Dvorkin and Nur, 1993).

Biot's main assumptions are: (i) seismic wavelengths are large in comparison to the dimensions of the macroscopic elementary volume; (ii) particle displacements are small in both the solid and the fluid; (iii) the liquid phase is continuous (disconnected pores are considered as part of the solid); (iv) the solid matrix is elastic, statistically isotropic, and homogeneous at microscopic scale; (v) the material is fully saturated; (vi) the response is computed at frequencies low enough that fluid flow can be described by Darcy's law; and (vii) gravity forces are neglected.

In Biot theory, wave propagation is described by two compressional waves and one shear wave. One kind of compressional wave is called the fast wave; it is similar to the P-wave in the nonporous elastic solid, and corresponds to a movement in which the solid and fluid displacements are in phase. The other kind of compressional wave is called the slow wave, and corresponds to a movement in which the solid and fluid displacements are out of phase (Bourbié et al., 1987).

Wave propagation in a statistically isotropic, heterogeneous poroelastic media is described by the equations (Biot, 1962):

$$\frac{\partial^2}{\partial t^2}\left(\rho u_i + \rho_f w_i\right) = 2\sum^{j}\frac{\partial}{\partial x_j}\left(\mu\varepsilon_{ij}\right) + \frac{\partial}{\partial x_i}\left(\lambda_c\varepsilon - \alpha M\zeta\right) \qquad (1a)$$

and

$$\frac{\partial^2}{\partial t^2}\left(\rho_f u_i + m w_i\right) = \frac{\partial}{\partial x_j}\left(\alpha M\varepsilon - M\zeta\right) - \frac{\eta}{k}\frac{\partial}{\partial t}w_i\,, \qquad (1b)$$

where the subscripts *i, j* = 1, 2 and 3 correspond to the *x*, *y* and *z* directions, respectively; $u_i$ is the displacement of the solid material; $w_i = \phi(v_i - u_i)$ is the displacement of the fluid relative to that of the solid, where $v_i$ is the displacement of the pore fluid; $\varepsilon_{ij}$ are the strain tensor of a porous solid; $\varepsilon$ is an invariant of the strain components identical to the volumetric strain; $k$ is the permeability of the porous medium; $\eta$ is the viscosity of the pore fluid; $\rho_f$ is the density of the pore fluid; $\rho$ is the overall density of the saturated medium; $m$ is the effective fluid density; $\mu$ and $\lambda_c$ are the Lamé parameters, $\mu$ being the shear modulus of the dry porous frame and $\lambda_c$ concerning the saturated medium; and $\alpha$ and $M$ are parameters related to the bulk moduli.

In the 2-D case, all the terms related to the *y* direction vanish:

$$\varepsilon_{ij} = \begin{bmatrix} \varepsilon_x & \frac{1}{2}\varepsilon_{xz} \\ \frac{1}{2}\varepsilon_{xz} & \varepsilon_z \end{bmatrix}, \tag{2}$$

$$\varepsilon_x = \frac{\partial u_x}{\partial x}, \tag{3}$$

$$\varepsilon_z = \frac{\partial u_z}{\partial z}, \tag{4}$$

$$\varepsilon_{xz} = \frac{\partial u_x}{\partial z} + \frac{\partial u_z}{\partial x}, \tag{5}$$

$$\varepsilon = \varepsilon_x + \varepsilon_z. \tag{6}$$

The overall density of the saturated medium is calculated from

$$\rho = \phi\rho_f + (1-\phi)\rho_s, \tag{7}$$

where $\rho_s$ is the density of the solid material and $\phi$ is the porosity. The effective fluid density is given by

$$m = T\rho_f / \phi, \tag{8}$$

where $T$ is the tortuosity,

$$T = 1 - r(1 - 1/\phi), \tag{9}$$

in which we consider solid spherical grains, $r = 0.5$ (Berryman, 1980). One must necessarily have $T \geq 0$.

The bulk modulus of the saturated medium, $K_c$, is defined similarly to the elastic case:

$$K_c = \lambda_c + \frac{2}{3}\mu. \tag{10}$$

According to Bourbié et al. (1987), in low porosity situations,

$$K_b = (1-\phi)K_s, \tag{11}$$

and Gassmann's equation (Gassmann, 1951) can be reduced to:

$$K_c = (1-\phi)K_s + \phi K_f, \tag{12}$$

where $K_b$ is the bulk modulus of the dry porous frame, $K_f$ is the bulk modulus of the pore fluid and $K_s$ is the bulk modulus of the solid material. $K_s$ and $K_f$ are determined directly from the input velocities and densities, by considering the situations $\phi = 0$ and $\phi = 1$, in equation (12), and using the formulae for the P-wave velocity of the saturated medium and the S-wave velocity, given respectively by

$$V_{P-c} = \sqrt{(K_c + 4\mu/3)/\rho} \tag{13}$$

and

$$V_S = \sqrt{\mu/\rho}. \tag{14}$$

The parameters $\alpha$ and $M$ are defined as

$$\alpha = 1 - K_b / K_s, \tag{15}$$

$$M = [\phi / K_f + (\alpha - \phi)/K_s]^{-1}. \tag{16}$$

**Formulation and computational aspects**

In order to implement the finite difference scheme, we reformulate equations (1) into

$$\left(m\rho - \rho_f^2\right)\frac{\partial U_x}{\partial t} = m\frac{\partial \tau_{xx}}{\partial x} + m\frac{\partial \tau_{xz}}{\partial z} + \rho_f\frac{\partial p_f}{\partial x} + \frac{\eta}{k}\rho_f W_x, \tag{17a}$$

$$\left(\rho_f^2 - m\rho\right)\frac{\partial W_x}{\partial t} = \rho_f\frac{\partial \tau_{xx}}{\partial x} + \rho_f\frac{\partial \tau_{xz}}{\partial z} + \rho\frac{\partial p_f}{\partial x} + \frac{\eta}{k}\rho W_x, \tag{17b}$$

$$\left(m\rho - \rho_f^2\right)\frac{\partial U_z}{\partial t} = m\frac{\partial \tau_{zz}}{\partial z} + m\frac{\partial \tau_{xz}}{\partial x} + \rho_f\frac{\partial p_f}{\partial z} + \frac{\eta}{k}\rho_f W_z, \tag{17c}$$

$$\left(\rho_f^2 - m\rho\right)\frac{\partial W_z}{\partial t} = \rho_f\frac{\partial \tau_{zz}}{\partial z} + \rho_f\frac{\partial \tau_{xz}}{\partial x} + \rho\frac{\partial p_f}{\partial z} + \frac{\eta}{k}\rho W_z, \tag{17d}$$

and

$$\frac{\partial \tau_{xx}}{\partial t} = \left(\lambda_c + 2\mu\right)\frac{\partial U_x}{\partial x} + \lambda_c\frac{\partial U_z}{\partial z} + \alpha M\left[\frac{\partial W_x}{\partial x} + \frac{\partial W_z}{\partial z}\right], \tag{18a}$$

$$\frac{\partial \tau_{xz}}{\partial t} = \mu\left[\frac{\partial U_x}{\partial z} + \frac{\partial U_z}{\partial x}\right], \tag{18b}$$

$$\frac{\partial p_f}{\partial t} = -\alpha M\left[\frac{\partial U_x}{\partial x} + \frac{\partial U_z}{\partial z}\right] - M\left[\frac{\partial W_x}{\partial x} + \frac{\partial W_z}{\partial z}\right], \tag{18c}$$

$$\frac{\partial \tau_{zz}}{\partial t} = \left(\lambda_c + 2\mu\right)\frac{\partial U_z}{\partial z} + \lambda_c\frac{\partial U_x}{\partial x} + \alpha M\left[\frac{\partial W_x}{\partial x} + \frac{\partial W_z}{\partial z}\right], \tag{18c}$$

where $U_i$ is the velocity of the solid material (first-time derivative of $u_i$), $W_i$ is the velocity of the fuid relative to that of the solid (first-time derivative of $w_i$), $\tau_{xx}$ and $\tau_{zz}$

are the normal stresses, $\tau_{xz}$ is the shear stress, and $p_f$ is the pore pressure.

Equations (17) and (18) are a first-order system of differential equations in velocity, stresses and pore pressure, which can be solved numerically by direct implementation of a finite-difference scheme. Then, based on Madariaga-Virieux staggered-grid formulation, we derived an explicit finite-difference approximation of these equations, which is second-order accurate time, fourth-order accurate space, the spatial operator being the Levander's difference formula (Madariaga, 1976; Virieux, 1984, 1986; and Levander, 1988).

Figure 1 shows the spatial distribution of the wave field components and poroelastic parameters on the staggered finite-difference grid.

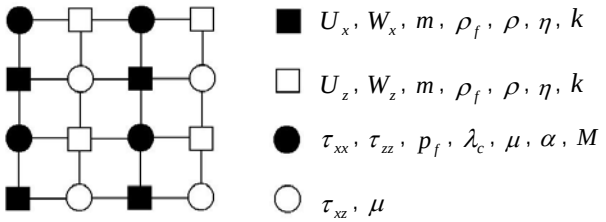


Figure 1 – Staggered grid. $U_x$ and $W_x$ are evaluated at $[i\Delta x, j\Delta z]$; $U_z$ and $W_z$ at $[(i+1/2)\Delta x, (j+1/2)\Delta z]$; $\tau_{xx}$, $\tau_{zz}$ and $p_f$ at $[(i+1/2)\Delta x, j\Delta z]$; and $\tau_{xz}$ is evaluated at $[i\Delta x, (j+1/2)\Delta z]$, where $\Delta x$ and $\Delta z$ are the grid increments; $i = 1,...,N_x$; $j = 1,...,N_z$; and $N_x$ and $N_z$ are the number of grid points in each direction.

The source function used in the algorithm is the second derivative of Gaussian wavelet,

$$F(t) = \{2\pi^3 (tf)^2 - 1\} \exp(-\pi^3 (tf)^2), \quad (19)$$

where $f$ is the dominant frequency (Cunha, 1997). In this work, we assume an explosive point source simply by adding the time function values $F(t)$, partitioned linearly between solid and fluid, as $(1-\phi)F(t)$ and $\phi F(t)$, respectively, to the solid normal stress components and pore fluid pressure component at the source grid point.

A nonreflecting boundary condition is incorporated into the four edges of the rectangular computational grid. We use a simple and robust scheme based on exponential reduction of the amplitudes in a strip of nodes along each boundary (Cerjan et al., 1985). In this case, the exponential factor is applied to the fields of velocities of the solid and of the fluid relative to those of the solid, and to the fields of stresses and pore pressure.

To keep grid dispersion down to an acceptable level, the following condition is used:

$$h \le V_{\min} / 5 f_{\max}, \quad (20)$$

where $V_{\min}$ is the minimum velocity involved in the computations; $f_{\max}$ is the maximum frequency; and $h$ is the grid spacing, assumed to be the same in both x and z directions. For numerical stability, the condition used is

$$\Delta t \le h / 5V_{\max}, \quad (21)$$

where $V_{\max}$ is the maximum velocity involved; and $\Delta t$ is the time sample.

The input parameters for the computations are $\phi$, $k$, $\eta$, $\rho_s$, $\rho_f$, $V_s$, $V_{P-s}$ (P-wave velocity of the solid material), and $V_{P-f}$ (P-wave velocity of the pore fluid).

**Experiments and results**

As initial tests (not shown here), we compared results from our algorithm with the ones published by Zhu and McMechan (1991), for a homogeneous model, by using the same poroelastic and computational parameters. The results were indistinguishable.

The numerical stability condition, given by equation (21), was sufficient until the viscosity to permeability ratio was $\eta/k \le 10^{+7}$ Pa*s/m$^2$. However, when $\eta/k = 10^{7+n}$ Pa*s/m$^2$, $n = 1,2,3,...$, we observed that the condition to avoid numerical instability becomes, approximately,

$$\Delta t \le 10^{-n} h / 5V_{\max}. \quad (22)$$

Figures 2 to 5 show synthetic seismograms for a homogeneous medium, at seismic (Figure 2 and 3) and sonic (Figure 4 and 5) frequencies. The poroelastic parameters are from Zhu and McMechan (1991, Table 1): $\rho_s$ = 2400 Kg/m$^3$, $\rho_f$ = 1000 Kg/m$^3$, $V_{P-s}$ = 2700 m/s, $V_S$ = 1500 m/s, $V_{P-f}$ = 1500 m/s, $\phi$ = 20 %, $k$ = 400 md. Several simulations are performed, and the effect of viscosity on wave propagation in poroelastic media is evaluated by changing this parameter in each simulation.

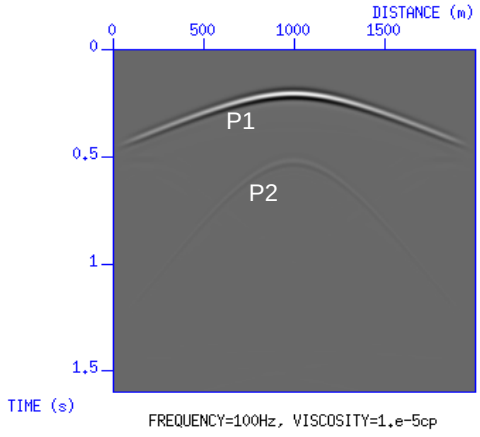


Figure 2 – Synthetic poroelastic seismogram of vertical solid velocity component. Viscosity is set to $10^{-5}$cp and frequency to 10 Hz. P1 is the direct P-wave (P1) and P2 is the slow wave (P2).

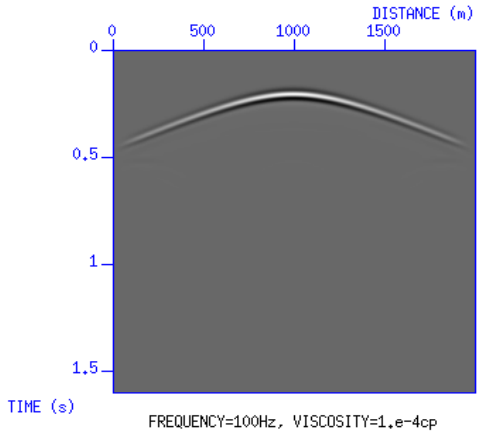


Figure 3 – Synthetic poroelastic seismogram of vertical solid velocity component. Viscosity is set to $10^{-4}$cp and frequency to 10 Hz.

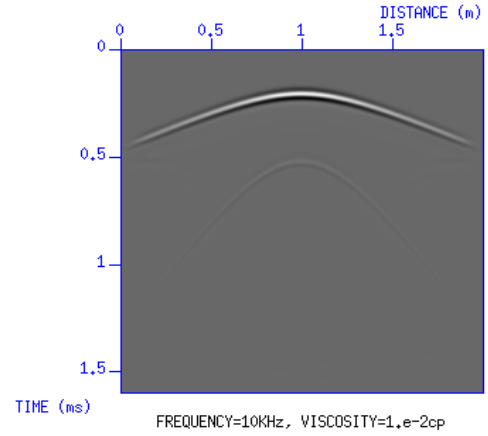


Figure 4 – Synthetic poroelastic seismogram of vertical solid velocity component. Viscosity is set to $10^{-2}$cp and frequency to 10 KHz.

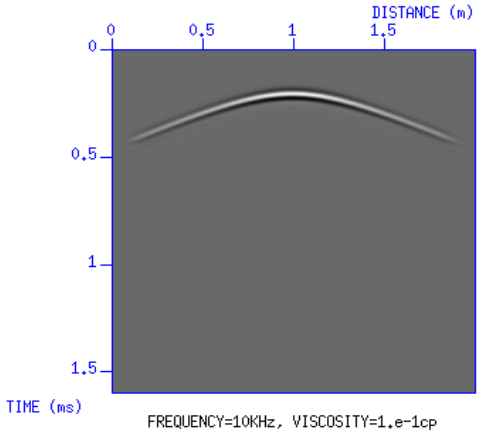


Figure 5 – Synthetic poroelastic seismogram of vertical solid velocity component. Viscosity is set to $10^{-1}$cp and frequency to 10 KHz.

For results showed in Figures 2 and 3, the source frequency is 10 Hz, the time sample is $4*10^{-4}$ s, the grid spacing is 5 m, the model dimension is 2000x2000 m, where receivers are disposed horizontally 200 m deep, and the source is at (1000, 600) m. For results showed in Figures 4 and 5, the frequency is 10 KHz, grid spacing is 0.005 m, the model dimension is 2x2 m, the receivers are disposed horizontally 0.2 m deep, and the source is at (1, 0.6) m. In the case of Figure 4, the time sample is $4*10^{-6}$ s and for Figure 5, it is $4*10^{-7}$ s. The nonreflecting boundary is applied in a strip width of 40 nodes in each edge.

We observe that, at 10 Hz, the slow wave is visible when the viscosity is, approximately, lower or equal to $10^{-5}$cp (Figure 2); when the viscosity is $10^{-4}$cp (Figure 3), the amplitude of the slow wave decreases to a level in which it is not visible any more. At 10 KHz, the slow wave is visible for viscosities until $10^{-2}$cp (Figure 4), but no more for $10^{-1}$cp (Figure 5).

The absence of S-wave in the Figures 2 to 5 indicates that the explosive source implemented here is sufficiently isotropic in the numerical grid.

Figure 6 represents a heterogeneous model, and its layers simulate some real media, such as shale and sandstone, saturated by water or gas. The appropriate parameters for such media are disposed in Table 1, and are based on data from Jones (1986); Dutta (1983); Dutta and Oddé (1983); Gregory (1977); and Norris (1989).

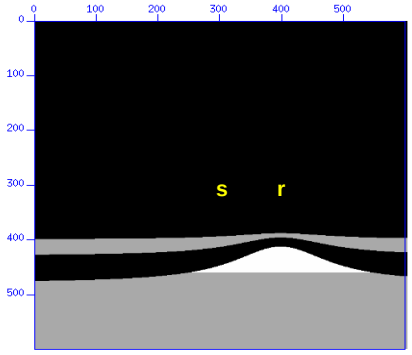


Figure 6 – An anticlinal sandstone reservoir model, where black represents shale, gray represents water-saturated sand, and white is for the gas-saturated sand. Parameters are listed in Table 1. The source position is indicated by “s” and receiver position is indicated by “r”.

In Table 1, the shale porosity is 16 %. However, for this kind of rock, most pores are isolated, and one of Biot’s assumptions considers such pores as part of solid material. Then, for shale, as input porosity in the simulations, we use the effective one, $\phi_{eff}$ = 0.1 %, and the input solid density is recalculated from

$$\rho_s^{eff} = (1-\phi_{isolada})\rho_s + \phi_{isolada}\rho_f \,, \qquad (23)$$

where $\phi_{isolated}$ is the isolated porosity, given by

$$\phi_{isolated} = \phi - \phi_{eff} \,. \quad (24)$$

Since the effective porosity is the one that contributes for the fluid movement, and it is too small, the effect of the relative movement between solid and fluid can be neglected in this case. Following this, we use an ideal value for shale permeability of 1 d, to avoid numerical instability. After these assumptions, all other input parameters are from Table 1 for modeling in the media showed in Figure 6.

Figure 7 shows results for simulations at seismic (100 Hz) and sonic (10 KHz) frequencies, respectively. For simulations at seismic frequency (Figure 7a), the time sample is $10^{-5}$ s, and the grid spacing is 1 m. For those at sonic frequency (Figure 7b), the time sample is $2*10^{-7}$ s, and the grid spacing is 0.01 m. In both cases, the model dimensions are 600x600 grid points, the source and receiver are located as indicated in Figure 5, and the nonreflecting boundary is applied in a strip width of 20 nodes, only in the left and right edges. Due to the geometry of the problem, the top and bottom reflections do not affect the results.

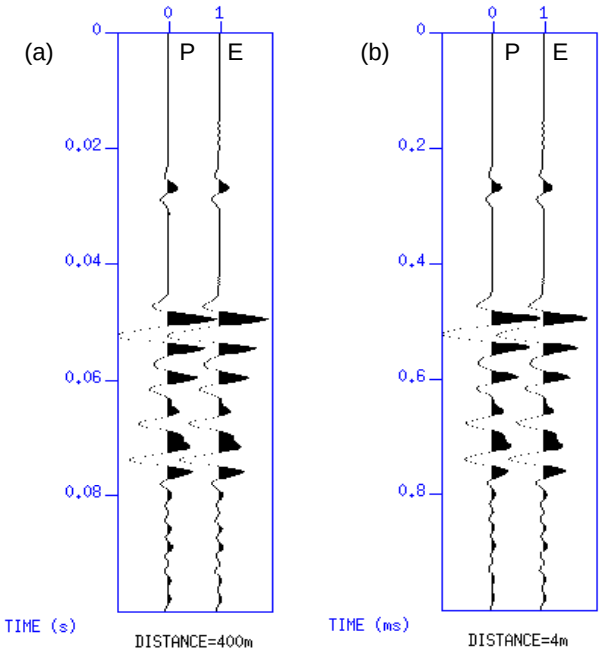


Figure 7 – Seismic (a) and sonic (b) traces recorded at the r-position in the model showed in Figure 6, illustrating the direct p-wave and primary and converted reflections from the fluid and lithologic interfaces. For each case, the first trace is from poroelastic modeling (P) and the second one is from elastic modeling (E).

When comparing results from elastic and poroelastic simulations, in Figure 7, we observe that, although there is no visible difference between the wave fields at the seismic frequency, for the sonic frequency, we observe a significant difference between the wave fields.

The poroelastic modeling is equivalent to the elastic one proposed by Levander (1988). For obtaining comparable results, we perform Levander's elastic modeling and use Gassmann's equation for converting poroelastic parameters into elastic ones. Obviously, the elastic modeling does not take into account the viscosity and permeability parameters.

**Discussion and synopsis**

The results above are predicted by Biot's theory, in which the behavior of the poroelastic medium can be significantly different for low and higher frequency ranges (Biot, 1956a, b; Bourbié et al., 1987; and Gurevich, 1996). Such difference is controlled by the parameter

$$r = f / f_c \,, \quad (25)$$

where $f$ corresponds to the source frequency and $f_c$ is the Biot's characteristic frequency, given by

$$f_c = \eta\phi / 2\pi k\rho_f \,. \quad (26)$$

When $r > 1$, the Biot's slow wave is relatively low attenuated, and it is significant in the overall energy balance of the wave field. When $r << 1$, the slow wave is a diffusive and highy attenuative wave, and all the Biot's poroelasticity effects are small. Bourbié et al. (1987) show that the slow wave effects can be neglected if $r < 0.15$.

The results showed in the Figure 7 correspond to $r \approx 1.6 \times 10^{-4}$ for the seismic frequency of 100 Hz, and to $r \approx 1.6$ for the sonic case (the gas saturated sandstone parameters are used for calculating $f_c$). That's the reason for the poroelasticity effect not to be visible in the seismic range when the poroelastic and elastic results are compared (Figure 7a). On the other hand, the effects of Biot's poroelasticity are significant at sonic frequency (Figure 7b), and the use of this wave propagation theory may provide valuable results in acoustic log inversion.

Although in most cases at seismic frequencies the Biot's poroelasticity effects are not significant, in some situations, such as highly heterogeneous media, the cumulative effect may conduce to noticeable differences (Hassanzadeh, 1991; Norris, 1993; and Gurevich and Lopatnikov, 1995).

**Acknowledgments**

This research was supported primarily by PETROBRAS, and additional support was provided by ANP.

**References**

Berryman, J. G., 1980, Long-wavelength propagation in composite elastic media, I. spherical inclusions: J. Acoust. Soc. Am., 68, 1809-1819.

Biot, M. A., 1956a, Theory of propagation of elastic waves in a fluid-saturated porous solid. I. Low-frequency range: J. Acoust. Soc. Amer., 28, 168-178.

------ 1956b, Theory of propagation of elastic waves in a fluid-saturated porous solid. II. Higher-frequency range: J. Acoust. Soc. Amer., 28, 179-191.

------ 1962, Mechanics of deformation and acoustic propagation in porous media: J. App. Phys., 33, 1482-1498.

Bourbié, T., Coussy, O., and Zinszner, B., 1987, Acoustics of porous media: Gulf Publishing Co.

Cerjan, C., Kosloff, D., Kosloff, R. and Reshef, M., 1985, A nonreflecting boundary condition for discrete acoustic and elastic wave equations: Geophysics, 50, 705-708.

Cunha, P. E. M., 1997, Estratégias eficientes para migração reversa no tempo pré-empilhamento 3-D em profundidade pelo método das diferenças finitas: MSc dissertation, Universidade Federal da Bahia.

Dai, N., Vafidis, A., and Kanasewich, R., 1995, Wave propagation in heterogeneous, porous media: A velocity-stress, finite-difference method: Geophysics, 60, 327-340.

Dutta, N. C., 1983, Shale compaction and abnormal pore pressure: A model of geopressures in the Golf Coast Basin: 53rd Ann. Internat. Mtg., Soc. Expl. Geophys., Expanded Abstracts, 542-544.

Dutta, N. C., and Odé, H., 1979, Attenuation and dispersion of compressional waves in fluid filled porous rocks with partial gas saturation (White model) – Part II: Results: Geophysics, 44, 1789-1805.

Dvorkin, J., and Nur, A., 1993, Dynamic poroelasticity: A unified model with the squirt and the Biot mechanism: Geophysics, 58, 524-533.

Gassmann, F., 1951, Uber die elastizitat poroser medien: Verteljahrsschrift der Naturforschenden Gesellschaft in Zurich, 96, 1-23.

Gregory, A. R., 1977, Aspects of rock physics from laboratory and log data that are important to seimic interpretation in seismic stratigraphy – application to hydrocarbon exploration: Am. Assn. Petr. Geol., Memoir 26, 15-46.

Gurevich, B., 1996, On: "Wave propagation in heterogeneous, porous media: A velocity-stress, finite-difference method" by Dai, Vafidis and Kanasewich (Geophysics, 60, 327-340): Geophysics, 61, 1230-1232.

Gurevich, B., and Lopatnikov, S. L., 1995, Velocity and attenuation of elastic waves in finely layered porous rocks: Geophys. J. Internat., 121, 933-947.

Hassanzadeh, S., 1991, Acoustic modeling in fluid-saturated porous media: Geophysics, 56, 424-435.

Jones, T. D., 1986, Pore fluids and frequency-dependency wave propagation: Geophyisics, 51, 1939-1953.

Levander, A. R., 1988, Fourth-order finite-difference P-SV seismograms: Geophysics, 53, 1425-1436.

Madariaga, R., 1976, Dynamics of an expanding circular fault: Bull. Seis. Soc. Am., 66, 639-666.

Mavko, G. and Nur, A., 1975, Melt squirt in the asthenosphere: J. Geophys. Res., 80, 1444-1448.

Mavko, G. and Nur, A., 1979, Wave attenuation in partially saturated rocks: Geophysics, 44, 161-178.

Norris, A., 1989, Stoneley wave attenuation and dispersion in permeable formations: Geophysics, 54, 330-341.

Norris, A. N., 1993, Low-frequency dispersion and attenuation in partially saturated rocks: J. Acoust. Soc. Amer., 94, 359-370.

O'Connell, R. J. and Budiansky, B., 1977, Viscoelastic properties of fluid-saturated cracked solids: J. Geophys. Res., 82, 5719-5736.

Rosenbaum, J. H., 1974, Synthetic microseismograms: Logging in porous formations: Geophysics, 39, 14-32.

Virieux, J., 1984, *SH*-wave propagation in heterogeneous media: Velocity-stress finite-difference method: Geophysics, 49, 1933-1957.

------ 1986, *P-SV*-wave propagation in heterogeneous media: Velocity-stress finite-difference method: Geophysics, 51, 889-901.

Zhu, X., and McMechan, G. A., 1991, Numerical simulation of seismic responses of poroelastic reservoirs using Biot theory: Geophysics, 56, 328-339.

Table 1 – Poroelastic parameters for the model showed in Figure 6.

| | Shale/water | Sand/water | Sand/gas |
|---|---|---|---|
| P-wave velocity of solid | 4 790 m/s | 5 450 m/s | 5 450 m/s |
| S-wave velocity | 2 520 m/s | 3 250 m/s | 3 250 m/s |
| P-wave velocity of fluid | 1 500 m/s | 1 500 m/s | 630 m/s |
| Density of solid | 2 680 Kg/m$^3$ | 2 630 Kg/m$^3$ | 2 630 Kg/m$^3$ |
| Density of fluid | 1 000 Kg/m$^3$ | 1 000 Kg/m$^3$ | 140 Kg/m$^3$ |
| Porosity | 16 % | 25 % | 25 % |
| Permeability | 0.0014 md | 1 d | 1 d |
| Viscosity of fluid | 1 cp | 1 cp | 0.022 cp |